

Variability and Unification of Blazars and Gamma Ray Bursts

Charles D. Dermer & James Chiang

*Naval Research Laboratory, Code 7653, Washington, DC 20375-5352
USA*

Abstract. Most models for blazars and gamma-ray bursts involve relativistic plasma outflows powered by accretion processes onto black holes. The blast wave physics developed for cosmological models of GRBs is reviewed. Two points relevant for blazar modeling are made: (1) The injection of nonthermal relativistic particles in the comoving frame is simply treated though a process of energizing the plasma as it sweeps up material from the surrounding medium. (2) The primary energy source of blazar radiation derives from the bulk kinetic energy of the outflowing plasma. Thus deceleration of the plasma blast wave must be included in blazar flaring calculations, and this process will introduce temporal and spectral effects in addition to those produced by acceleration and radiative cooling.

1. Introduction

The purpose of this paper is to provide an introductory review of the blast wave physics developed to model prompt and afterglow GRB emissions, with an eye toward using these tools in blazar modeling. When constructing such models, an important difference between the blazar and burst systems that should be kept in mind is that blazars involve continuous accretion processes which expel plasma with initial bulk Lorentz factors (or baryon-loading factors) $\Gamma_0 \lesssim 30$. In contrast, GRBs originate from one-time catastrophic accretion events which drive plasma outflows with $\Gamma_0 \sim 300$. Thus a blazar spectrum could result from a superposition of injection events, whereas this is less likely to be the case for GRBs unless the central source ejects successive shells.

The blazar category refers collectively to several different classes of sources which are defined according to specific observational criteria, and includes flat spectrum radio quasars, highly polarized quasars, optically violently variable quasars, and BL Lac objects. Most models interpret the properties of these classes in view of the circumstance that our line-of-sight is aligned nearly along the direction of a jet of relativistic plasma expelled from a central engine; thus it has proven useful to adopt the common designation blazar.

The gamma-ray observations indicate extremely large *apparent* blazar luminosities, attaining values $L_\gamma \sim 10^{48} \Delta\Omega_j$ ergs s^{-1} in some sources (e.g., Hartman et al. 1997; Mattox et al. 1997). The actual luminosity is reduced from the apparent luminosity due to jet collimation. If the parent population of blazars are radio galaxies (e.g., Urry & Padovani 1995), then jet beaming fac-

tors $\Delta\Omega_j/4\pi \cong 10^{-2}$ - 10^{-3} are implied by observations, so that $L \lesssim 10^{46}$ - 10^{47} ergs s^{-1} . One-day flares therefore involve energy releases as large as $E \sim 10^{52}$ ergs.

GRBs involve very large, impulsive energy releases. In the case of GRB 971214 with a candidate host galaxy at redshift $z = 3.42$ (Kulkarni et al. 1998), the apparent gamma-ray luminosity $L_\gamma \sim 10^{52}$ ergs s^{-1} . The gamma-ray luminous phase lasted for ~ 40 s (Kippen et al. 1997). Taking into account the afterglow radiation, this implies an apparent total energy release of $E \sim 10^{54}$ ergs. Models of both blazar flares and GRB events therefore deal with energies per solid angle $\partial E/\partial\Omega \sim 10^{53}$ ergs sr^{-1} . Unlike blazars, whose outflows are thought to be driven by accretion onto supermassive black holes, the mechanism producing GRBs remains controversial.

Our primary channel of information about blazars and GRBs derives from the nonthermal radiation produced by the relativistic plasma expelled from a central engine. As indicated above, the total energy release and energy-release time scales constitute the most important observables, though determinations of E are uncertain to the extent that the outflow is collimated. The next most important quantity to characterize the explosion physics and nature of the source is the baryon-loading factor, which is also referred to as the entropy per baryon. This quantity represents the mean energy of a baryon after the fireball has become optically thin (see, e.g., Mészáros & Rees 1993; Piran 1994), and is essentially equivalent to the initial Lorentz factor Γ_0 of the bulk outflow.

In what follows, we review the physics that has been developed to analyze GRB observations, and indicate how these results can be applied to blazar research and other systems which produce relativistic plasma outflows. By characterizing the properties of these outflows, we hope to determine the nature of the sources which expel highly relativistic plasma.

2. Fireball and Blast Wave Physics

If a mass M_{baryon} of baryons is mixed in the explosion energy, then the resulting fireball will expand and transfer most of its energy to baryons, ultimately producing a relativistic outflow moving with Lorentz factor

$$\Gamma_0 \simeq \frac{E_{\text{tot}}}{M_{\text{baryon}}c^2}. \quad (1)$$

Observations of superluminal motion in radio-loud AGNs reveal parsec-scale relativistic plasma outflows moving with a wide range of Γ_0 , though rarely exceeding $\Gamma_0 \sim 20$ - 30 (e.g., Vermeulen & Cohen 1994). An outstanding question in black hole research is the nature of the processes which expel relativistic plasma. Many mechanisms have been suggested, including the Blandford-Znajek (1977) process for extracting black hole rotational energy through magnetic couplings between the accretion disk and black hole. The large radiant luminosities of accreting black holes have also been suggested to drive hot plasma to relativistic energies through the Compton rocket effect (e.g., O’Dell 1981; Phinney 1982), or to slow very high energy particles through Compton drag (Melia & König 1989). Stochastic accretion with accompanying diffusive escape of high-energy

protons and electrons has also been proposed (Dermer, Miller, & Li 1996) as a source of outflows from accreting black holes.

As already mentioned, the nature of the central engine which drives the relativistic outflows from GRB sources is unclear. It is interesting to note that if we assume the emission is uncollimated in GRB 971214 and that $\Gamma_0 = 300\Gamma_{300}$ with $\Gamma_{300} \sim 1$, then only a Jupiter's mass of baryons is mixed into an energy release $\gtrsim 100$ times the entire energy that the Sun will radiate over its lifetime. This circumstance requires an extraordinarily baryon-free environment. The explanation of these incredibly energetic outflows is one of the outstanding contemporary problems in astronomy. Widely discussed GRB triggers include coalescence of compact objects (e.g. Mészáros, & Rees 1992), the collapse of massive stars (Paczynski 1998), and failed supernovae or collapsars (Woosley 1993).

2.1. Special Relativity

Special relativity plays a key role in spectral calculations of relativistic plasma outflow. The most important effects include the relativistic boosting of the radiation, which is primarily governed by the value of the Doppler factor $\mathcal{D} = [\Gamma(1 - B\mu)]^{-1}$, where $B = \sqrt{1 - \Gamma^{-2}}$ and $\arccos \mu$ is the angle between the observer and the direction of motion of the radiating element. The Doppler boosting means that most of the observed radiation is emitted from angles

$$\theta \lesssim 1/\Gamma. \quad (2)$$

A second important effect is that during the time interval Δt over which an observation takes place, the plasmoid traverses a distance

$$\Delta x \cong \Gamma^2 c \Delta t / (1 + z). \quad (3)$$

A third effect is the strong reduction of the comoving luminosity L' by a factor $\sim \Gamma^4$ in comparison with the luminosity that would be inferred if the radiating plasma is assumed to be at rest with respect to the observer. If $J(\epsilon')$ (ergs $\text{s}^{-1} \epsilon'^{-1}$) is the spectral emissivity at comoving dimensionless photon energy $\epsilon' = h\nu'/(m_e c^2)$, then

$$\nu L_\nu = \mathcal{D}^4 \epsilon' J(\epsilon') \sim \Gamma^4 L'. \quad (4)$$

These effects are well-known when Γ is constant (see, e.g., Begelman et al. 1984, Dermer et al. 1997). Variations of Γ with distance (or time) will complicate these relations. Much of the new physics being studied as a result of GRB observations has to do with observable consequences resulting from deceleration of the relativistic outflows.

The effect described by eq.(4) resolves the $\gamma\gamma$ transparency problem in blazars and GRBs. If the emitting region were stationary with a size $R \sim c\Delta t_{\text{var}}/(1 + z)$ implied by the variability time scale Δt_{var} , then γ -rays could not escape due to attenuation by the process $\gamma + \gamma' \rightarrow e^+ + e^-$ (Baring & Harding 1997; Maraschi et al. 1992). Given the rapid variability of the radiation, either beaming of the radiation or bulk relativistic outflows are therefore required to explain the detection of gamma rays. Depending on the specific GRB and the observing time, the emitting regions of GRBs must be moving with $\Gamma_0 \gtrsim 30$ -100 in order to be transparent to gamma rays.

2.2. Deceleration Radius and Time Scale

As relativistic plasma expands into the surrounding medium, its entrained magnetic field sweeps up and captures electrically-charged particles. These particles enter the comoving fluid frame with Lorentz factor Γ to provide a source of free energy which becomes available to be radiated. The strength of the plasma magnetic field necessary to capture particles is determined by the condition that the Larmor radius is less than the width of the plasmoid or blast wave. Here we distinguish the use of the terms “plasmoid” and “blast wave.” Plasmoid refers to any coherent plasma outflow that can be treated as a hydrodynamical fluid. The plasmoid cross-sectional area which is effective at sweeping up particles is $A(x) \propto f(x)\delta\Omega$, where $f(x)$ can be specified generally and x is a spatial coordinate. By contrast, a blast wave is a type of plasmoid which expands according to the rule $A(x) \propto x^2$. Henceforth we consider blast waves, keeping in mind that the results can be straightforwardly extended to the more general plasmoid geometry.

The total mass which is swept-up by the plasma as it travels a distance δx is simply $m_p n(x)A(x)\delta x$, where $n(x)$ is the density of the particles in the surrounding medium, which we suppose to be composed of hydrogen. Each proton and electron captured from the surrounding medium carries a relativistic energy $\Gamma m_p c^2$ into the comoving fluid frame. The blast wave no longer coasts but decelerates when the incoming relativistic inertia equals the rest mass energy of the ejecta, that is, when $V_d m_p \Gamma_0 c^2 = E/(\Gamma_0 c^2)$, where the deceleration volume $V_d = 4\pi x_d^3/3$. Hence the deceleration radius is given by

$$x_d = \left(\frac{3E}{4\pi n_0 \Gamma_0^2 m_p} \right)^{1/3} \cong 2.6 \times 10^{16} \left(\frac{E_{54}}{n_2 \Gamma_{300}^2} \right)^{1/3} \text{ cm} \quad (5)$$

(Rees & Mészáros 1992), where $n_0 = 10^2 n_2 \text{ cm}^{-3}$ is the density at x_d , the explosion energy $E = 10^{54} E_{54}$ ergs, and we assume a uniform density $n(x) = n_0$.

The strongly Doppler-beamed emission from a relativistically expanding shell means that only that portion of the blast wave found within an angle $\sim 1/\Gamma_0$ to the line-of-sight produces much of the prompt GRB emission. In the frame of the observer, the emitting region is chasing its photons and keeping close behind them, at least when $\Gamma/\Gamma_0 \sim 1$. The $(1 - B\mu)$ factor in the Doppler effect means that the deceleration time scale t_d of the blast-wave, as measured by an observer, is given by

$$t_d = \frac{(1+z)x_d}{\Gamma_0^2 c} \cong 9.6(1+z) \left(\frac{E_{54}}{n_2 \Gamma_{300}^8} \right)^{1/3} \text{ s}. \quad (6)$$

2.3. Radiative Regimes

The equation of motion of the blast wave depends on the amount of internal energy it radiates. The adiabatic regime applies to the case where very little of its internal energy is radiated, and the radiative regime applies when essentially all of its internal energy is radiated on a time scale short compared with the deceleration time scale as measured in the comoving frame. In the former case, we can write the equation of momentum conservation as

$$B\Gamma M_{\text{baryon}} + (B\Gamma) \cdot \Gamma \cdot \left(\frac{4\pi}{3} m_p n_0 x^3 \right) = B_0 \Gamma_0 M_{\text{baryon}}. \quad (7)$$

When $x \gg x_d$,

$$\Gamma_{\text{adi}} \propto x^{-3/2} \quad (8)$$

(Blandford & McKee 1976). In the latter (radiative) case, the momentum conservation equation is the same as given in eq. (7), except that the weighting factor Γ in the second term on the left-hand-side is replaced by unity, because all the internal energy is promptly radiated away. Thus we find that when $x \gg x_d$,

$$\Gamma_{\text{rad}} \propto x^{-3} . \quad (9)$$

In general,

$$\Gamma_{\text{rad}} \propto x^{-g} , \text{ with } 3/2 < g < 3 . \quad (10)$$

The range of g specified in eq.(10) applies to the case of a uniform density surrounding medium.

2.4. Properties of the Relativistic Plasma

The baryons initially mixed in the explosion adiabatically expand until the initial explosion energy is transformed into directed plasma kinetic energy. In the comoving fluid frame, the baryons become nonrelativistic. Particles which are swept-up from the surrounding medium with Lorentz factor Γ in the comoving frame provide a source of free energy which is derived from the bulk kinetic energy. This causes the blast wave to decelerate, and the Doppler boosting becomes weaker. Both nonthermal electrons and protons are swept up, but because of the greater mass of the protons, most of the free energy is initially in the form of nonthermal protons. Other than to simply heat the thermal plasma or escape, the only known way to radiatively dissipate this energy efficiently is by transferring a large fraction of the nonthermal proton energy to nonthermal electrons.

A nonthermal proton could in principle transfer nearly all its energy to a very energetic electron. This maximum defines a minimum Lorentz factor $\gamma_{e,\text{min}}$ carried by a swept-up electron, noting that Fermi processes in the blast wave could further accelerate the nonthermal electrons to $\gamma \gg \gamma_{e,\text{min}}$. Thus

$$\gamma_{e,\text{min}} = \xi_e (m_p/m_e) \Gamma , \quad (11)$$

where the electron equipartition factor $\xi_e \lesssim 1$.

A central uncertainty in blast wave physics is the magnetic field strength in the comoving fluid frame. A convenient way to characterize the blast wave magnetic field H is through the prescription

$$\frac{H^2}{8\pi} \cong (4\Gamma n_0) (\Gamma m_p c^2) \xi_H , \quad (12)$$

where the right hand side represents the energy density of the swept-up electron-proton fluid downstream of the blast wave shock. Note that the particle density is enhanced by Lorentz contraction, and that the compression ratio factor r is normalized to the factor of 4 which represents an important limit in nonrelativistic shock theory (a more realistic value of r would be 7, given that the

downstream particles constitute a relativistic fluid). The term ξ_H is the magnetic equipartition parameter. Thus

$$H \cong 120 \Gamma_{300} n_0^{1/2} \xi_H^{1/2} \text{ Gauss} . \quad (13)$$

The relativistic electrons in the blast-wave plasma will radiate nonthermal synchrotron radiation with frequencies $\nu_p[\text{Hz}] \gtrsim 3 \times 10^6 H \gamma_{e,\text{min}}^2 \propto \Gamma_{300}^3 \xi_H^{1/2} \xi_e^2$ in the blast-wave frame. If the index p of the electron number spectrum is steeper than 3, this frequency represents the peak of the measured νF_ν spectral energy distribution produced by nonthermal electron synchrotron. Other spectral components, in particular the synchrotron self-Compton (SSC) and the nonthermal proton synchrotron emissions, will also be radiated, but are usually found (Chiang & Dermer 1998; Panaitescu & Mészáros 1998; Böttcher & Dermer 1998) to be energetically less important than the nonthermal electron synchrotron luminosity during the prompt gamma-ray luminous phase of a GRB.

2.5. Sweeping Energization

The conversion of the bulk kinetic energy of the plasma outflow to nonthermal particle and magnetic-field energy in the comoving frame involves very complicated plasma physics and shock acceleration processes. If this energy is extracted through the process of sweeping-up material from the surrounding medium, the detailed acceleration physics can fortunately be avoided by simply assuming that some fraction of the initial swept-up energy is transformed into a distribution of nonthermal electrons with a minimum energy given by eq.(11).

The correct description of the plasmoid dynamics must take into account the changing internal energy content and inertia of the plasmoid as it sweeps up matter from the external medium. The momentum distribution of the swept-up energetic particles evolves through subsequent acceleration, radiative losses, and particle escape. This causes the inertia of the plasmoid to change, thereby affecting its subsequent dynamics. The important point to note is that *the energy of the nonthermal particle distribution function in the comoving frame derives ultimately from the directed bulk kinetic energy of the plasma outflow; thus models for GRBs and blazar flares must include effects of plasmoid deceleration.*

An equation which explicitly couples the plasmoid dynamics with the comoving particle distribution function was derived from momentum conservation by Dermer & Chiang (1998), and is given by

$$-\frac{[\partial P(x)/\partial x]}{P(x)} = \frac{n_{\text{ext}}(x)A(x)\Gamma(x)(1 + m_e/m_p)}{N_{\text{th}}(1 + a_{\text{th}}) + \int_0^\infty dp \gamma [N_{\text{pr}}(p; x) + a_{\text{nt}}N_e(p; x)]} . \quad (14)$$

Here $p = \beta\gamma$ is the dimensionless momenta of the protons or electrons whose momentum distribution functions are denoted by the subscript “pr” or “e”, respectively, and $P = B\Gamma$ is the dimensionless momentum of the plasmoid. In eq.(14), only protons and electrons are considered, though the result is easily generalized for heavier ions and pairs. This expression represents the inverse of the characteristic length scale over which the plasmoid decelerates. The rate of spatial deceleration is impeded by the relativistic inertia of the plasmoid, which is given by the two terms in the denominator on the right-hand-side. The first

term represents the number of thermal protons multiplied by a weighting factor which corrects for thermal electrons or pairs. If only electrons are present, $a_{\text{th}} = m_e/m_p$. The second term in the denominator in the form of an integral represents the relativistic inertia given through the nonthermal proton and electron distribution functions. Again, if no pairs are present, $a_{\text{nt}} = m_e/m_p$. The numerator on the right-hand-side of eq.(14) is proportional to the spatial momentum impulse applied to the plasmoid through the process of sweeping-up particles from the external medium.

Eq.(14) is amenable to a variety of analytic treatments, and can easily be shown to yield the adiabatic and radiative limits previously considered. An analytic solution is possible for a plasmoid with a constant entrained magnetic field which decelerates by sweeping up material from a smooth external medium with density $n_{\text{ext}}(x) \propto x^{-\eta}$ (Dermer & Chiang 1998). There we showed that GRB afterglows exhibit two temporal and spectral regimes, depending on whether synchrotron cooling plays a negligible or major role in the cooling of the bulk of the electrons that produce radiation at a given energy. If the flux density is written in the form $S(\epsilon, t) = \epsilon \dot{N}(\epsilon, t) = K t^{-\chi} \epsilon^{-\alpha}$, then in the uncooled regime $\alpha_{\text{uncooled}} = (s - 1)/2$, where s is the injection index of electrons, and

$$\chi_{\text{uncooled}} = \frac{g(3 + s) - 2(j + 1 - \eta)}{2(2g + 1)} \rightarrow \frac{g(s + 3) - 6}{2(2g + 1)}. \quad (15)$$

In the cooled regime, $\alpha_{\text{cooled}} = s/2$ and

$$\chi_{\text{cooled}} = \frac{g(s + 6) + 2 - 2(j + 1 - \eta)}{2(2g + 1)} \rightarrow \frac{g(s + 6) - 4}{2(2g + 1)}. \quad (16)$$

The transition from the uncooled to the cooled regime occurs at the observer time

$$t_{\text{tr}} \simeq \frac{5(1 + z)^{0.38}}{H_0^{1.85} \epsilon^{0.62}} \text{ sec} \quad (17)$$

(see eqs. 52-54 in Dermer & Chiang 1998), where ϵ is the observed dimensionless photon energy and H_0 is the magnetic field strength in Gauss, assumed constant in time. The expressions on the rhs of eqs.(15) and (16) apply to a blast-wave geometry (i.e., $A(x) \propto x^j$ with $j = 2$) and a uniform density ($\eta = 0$) medium.

It is a simple matter to show that if the X-ray afterglows are observed in the cooled regime, as is likely, then injection indices $s \cong 2$ and radiative indices in the range $3/2 \lesssim g \lesssim 3$ imply $1.0 \lesssim \chi \lesssim 10/7 = 1.43$. This reproduces the range of temporal indices observed in GRB X-ray afterglows, which are generally well fit by χ in the range $1.1 \lesssim \chi \lesssim 1.5$ (e.g. Costa et al. 1997; Feroci et al. 1998; Piro et al. 1998). This analytic treatment (see also Sari, Piran, & Narayan 1998; Wijers et al. 1997) makes several predictions, most importantly that during the transition from the uncooled to the cooled regime, the photon spectral index changes by 1/2 unit and the temporal index changes in value according to eqs.(15) and (16).

Eq.(14) can also be used to make estimates for the temporal and spectral behavior associated with sweeping energization and blast wave deceleration by other radiation processes. For example, very high energy protons will produce nonthermal synchrotron radiation (Vietri 1997). Because the protons radiate

very inefficiently, they are, in general, not strongly cooled, in which case the emission from this process can be shown (Böttcher & Dermer 1998) to decay more slowly than electron synchrotron or SSC radiation. Temporal decay indices for proton synchrotron radiation from uncooled protons in a constant magnetic field are given by eq.(15); the indices in the uncooled synchrotron case for a magnetic field which varies according to eq.(13), with ξ_H constant, are given by (Böttcher & Dermer 1998).

2.6. Blast Wave Deceleration

In blazar physics, nonthermal electrons are normally injected either impulsively or over some fixed interval of time in the comoving frame. The effects of particle acceleration or cooling processes are then calculated and used to model the multiwavelength spectral energy distributions, or to characterize observations of spectral variability. Blast wave physics shows how the injection problem can be solved, namely by extracting energy from the bulk relativistic motion of the plasmoid and transforming it into nonthermal particle energy, making sure that momentum conservation is satisfied. The major uncertainty in following this prescription is to specify the density distribution of the surrounding medium which is intercepted and swept-up by the plasmoid. A more comprehensive calculation, beyond the one-component description discussed here, should also take into account radiation from the reverse shock (see, e.g., Panaitescu, & Mészáros 1998) and light-travel time effects from injection into different portions of a plasmoid or blast wave with finite extent.

The discussion in the previous section illustrates the importance of treating particle injection and blast wave deceleration on equal footing. For example, a decaying time profile cannot be simply interpreted as a decrease in the number of radiating electrons through either cooling or losses. Because the injection of nonthermal particles is accompanied by plasmoid deceleration, it is equally possible that the number of nonthermal particles increases, yet a decreasing flux is observed due to the slowing-down of the blast wave. In fact, this is the precisely the behavior that is evidently observed in GRBs at times $t > t_d$.

The interplay and importance of these effects are shown by models of X-ray observations of blazar sources such as Mrk 421 (Takahashi et al. 1996), OJ 287 (Idesawa et al. 1997), and PKS 2155-304 (Sembay et al. 1993). The X-ray data follow well-defined trajectories in the spectral index/flux plane. This behavior can be explained by synchrotron losses of nonthermal electrons which are injected into the comoving frame over a finite length of time (Dermer 1998; Kirk, Rieger, & Mastichiadis 1998). This behavior can also, however, be a consequence of the effects of plasmoid deceleration (Chiang 1998; Dermer, Li, & Chiang 1998). A related instance is the interpretations of energy-dependent lags from blazar flares. For example, the UV radiation lagged the X-ray emission in a flare from the BL Lac object PKS 2155-304 (Urry et al. 1994). This behavior could result from blast wave deceleration rather than from synchrotron losses.

3. Unification of Blazars and GRBs

Here we speak of unification in terms of the underlying physical processes which produce the radiation from the relativistic plasma outflows in blazars and GRBs.

The differences between the engines driving blazar and GRB outflows are obviously profound, but can be better investigated once the origin of these radiant emissions is established. Because blast wave physics has been used to successfully explain GRB afterglows, we argue that these tools should be equally applied to blazars.

Figs. 1 and 2 show calculations of the synchrotron and SSC radiation produced by uncollimated relativistic outflows which sweep up material from the surrounding medium, using the code developed by and described in Chiang & Dermer (1998). These calculations show spectra produced by uncollimated fireballs with total energy $E = 10^{54}$ ergs which are surrounded by a medium with uniform density $n_0 = 100 \text{ cm}^{-3}$. If the fireball is collimated into $\Delta\Omega_j$ sr, as might be the case for a blazar, then these calculations would equally represent the case where an observer was looking down a jet of material from a fireball where $10^{54} \Delta\Omega_j / (4\pi)$ ergs are injected, provided that the plasmoid area increased $\propto x^2$ and that the jet opening angle $\gg \Gamma_0^{-1}$.

Only two parameters differ between Figs. 1 and 2, namely Γ_0 and the fraction ξ of swept-up energy that is promptly channeled into nonthermal electrons. In Fig. 1, $\Gamma_0 = 200$ and $\xi = 0.1$, whereas in Fig. 2, $\Gamma_0 = 20$ and $\xi = 0.01$. In both calculations, $\xi_e = 1$ and $\xi_H = 10^{-5}$ (see Chiang & Dermer 1998 for reasons to assign this value in order to match GRB observations), the electron injection index $s = 3$, and γ ranges from $\gamma_{e,\min}$ given by eq.(11) to $\gamma_{e,\max} \cong 10^6 / \sqrt{H(\text{G})}$. This latter value is a theoretical upper limit determined by equating the time scale for an electron to execute a Larmor orbit with the synchrotron energy loss time scale.

Fig. 1 provides a reasonable representation of the typical spectral and temporal behavior of a “classical” GRB. The prompt emission, lasting for ~ 10 s (compare eq.[6]), is dominated by power emitted at gamma-ray energies. At later times, power-law X-ray and optical afterglows are found. The peak of the νF_ν spectrum moves to lower energies with time due to blast wave deceleration and synchrotron cooling. Two peaks in the spectral energy distribution are formed. The higher energy peak is formed from the SSC process, and produces late time GeV emission, as has been observed from GRBs (e.g., Hurley 1994).

As in the case of Fig. 1, Fig. 2 also shows a twin-peaked spectral energy distribution, which corresponds to the generic shape of the multiwavelength blazar spectra. The peak of the synchrotron component is now at X-ray energies rather than gamma-ray energies. The SSC component peaks at ~ 1 GeV - TeV energies. For this choice of parameters, the shortest flaring time scale is ≈ 1 hour due to the $\Gamma_0^{-8/3}$ dependence of t_d given by eq.(6). This overall behavior is in rough agreement with the flaring characteristics of BL Lac objects such as Mrk 421 and Mrk 501 (Macomb et al. 1995; Buckley et al. 1996; Catanese et al. 1997). A better comparison with the spectral energy distribution of X-ray selected BL Lacs might require that the upper energy of the electrons is less than the maximum value given by $\gamma_{e,\max}$.

4. Summary and Conclusions

New developments in our understanding of GRB sources appear to have much relevance for blazar modeling. Here we have tried to explain the basics of blast-

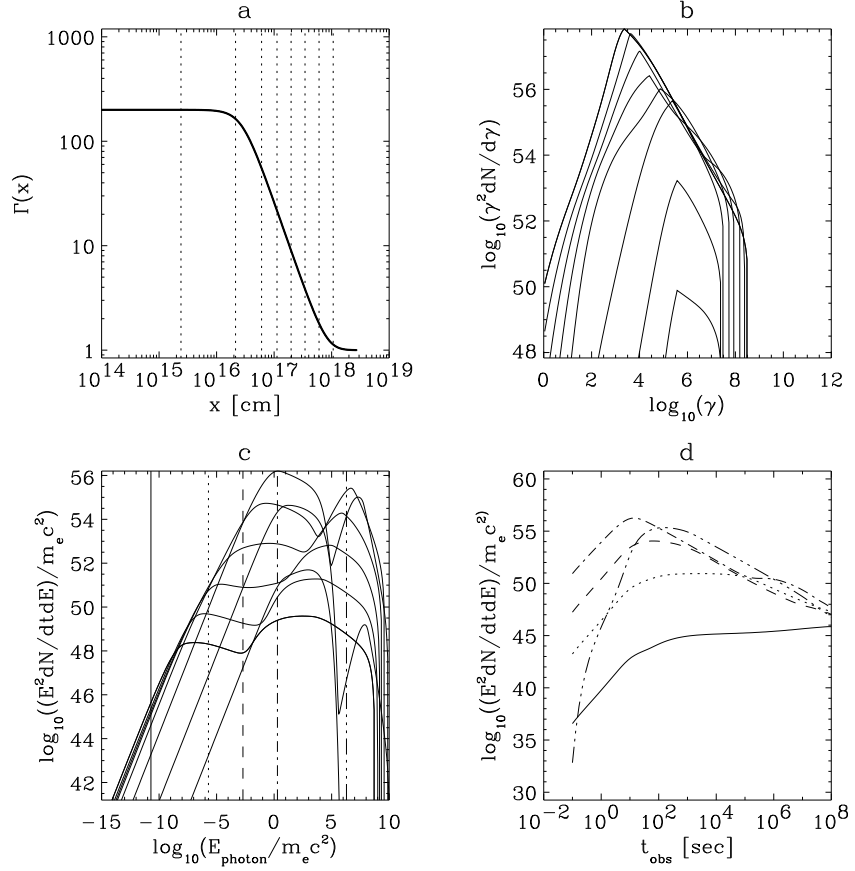


Figure 1. Calculations of blast wave deceleration and radiation for a fireball with energy $E = 10^{54}$ ergs and $\Gamma_0 = 200$, assuming that 10% of the swept-up nonthermal particle energy goes into nonthermal electrons. The dotted lines in panel a mark the Lorentz factors at observer times of 1 s, 10 s, 100 s, etc. Nonthermal electron spectra (panel b) and νL_ν photon spectra (panel c) are calculated in panels b and c, respectively. The respective Lorentz factors and times (Γ_0, t) for the electron and photon spectra are (200.0, 0.1 s), (199.8, 1.4 s), (122, 19.0 s), (36.9, 261.6 s), (13.2, 3600 s), (4.9, 5.0×10^4 s), (2.0, 6.8×10^5 s), and (1.14, 9.4×10^6 s). Panel d shows light curves at radio, optical, X-ray, MeV, and TeV energies. The shortest flaring time scale for this calculation is about 10 seconds at gamma-ray energies.

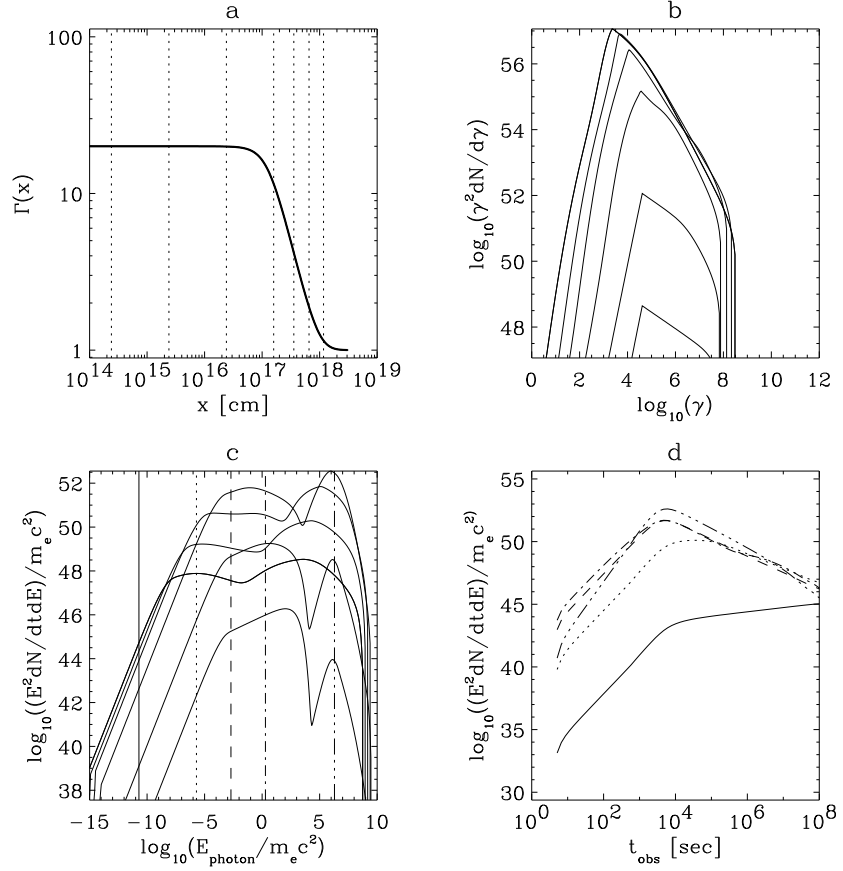


Figure 2. Calculations of blast wave deceleration and radiation for a fireball with $E = 10^{54}$ ergs and $\Gamma_0 = 20$, assuming that 1% of the swept-up nonthermal particle energy goes into nonthermal electrons. The dotted lines in panel a mark the Lorentz factors at observer times of 10 s, 100 s, 1000 s, etc. Nonthermal electron spectra (panel b) and νL_ν photon spectra (panel c) are calculated in panels b and c, respectively. The respective Lorentz factors and times (Γ_0, t) for the electron and photon spectra are (20.0, 19.0 s), (20.0, 262 s), (17.8, 3600 s), (5.5, 5.0×10^4 s), (2.1, 6.8×10^5 s), and (1.16, 9.4×10^6 s). Panel d shows light curves at radio, optical, X-ray, MeV, and TeV energies. The shortest flaring time scale for this calculation is about an hour at X-ray, gamma-ray and TeV energies.

wave physics, and to show how this approach can be straightforwardly applied to models of variability behavior in blazars. As illustrated in Figs. 1 and 2, models employing blast-wave physics qualitatively describe the overall spectral and temporal characteristics of GRBs and some X-ray selected BL Lac objects for which multiwavelength campaigns have been conducted. As higher quality X-ray and TeV observations become available, this model will provide specific predictions for correlated spectral and temporal behavior. Before applying our model to flat spectrum radio quasars, however, extensions of this work to deal with external radiation fields must be included.

The central point made here is that blazar flares are a result of the conversion of directed plasma energy into internal nonthermal particle energy. Energization of the nonthermal protons and electrons comes at the expense of the directed kinetic energy of the relativistic outflow. Associated blast-wave deceleration must therefore be treated when modeling blazar flares. Blazars and GRBs display overall similarities in terms of their spectral energy distributions. To first order, blazars differ from GRBs by ejecting plasma with \sim an order-of-magnitude less entropy per baryon. Why this should be so is unknown, and represents a significant clue and a strong constraint on any models for the underlying engines.

5. Acknowledgments

Useful discussions with M. Böttcher are acknowledged. The work of JC was performed while he held a National Research Council - Naval Research Laboratory Associateship. The work of CD is supported by the Office of Naval Research.

References

- Baring, M. G., & Harding, A. K. 1997, *ApJ*, 491, 663
 Begelman, M. C., Blandford, R. D., & Rees, M. J. 1984, *RMP*, 56, 255
 Blandford, R. D., & McKee, C. F. 1976, *Phys. Fluids*, 19, 1130
 Blandford, R. D., & Znajek, R. L. 1977, *MNRAS*, 179, 433
 Böttcher, M., & Dermer, C. D. 1998, *ApJ*, 499, L131
 Buckley, J. H. et al. 1996, *ApJ*, 472, L9
 Catanese, M., et al. 1997, *ApJ*, 487, L143
 Chiang, J., & Dermer, C. D. 1998, *ApJ*, in press (astro-ph/9803339)
 Chiang, J. 1998, *ApJ*, in press (astro-ph/9805302)
 Costa, E., et al. 1997, *Nature*, 387, 783
 Dermer, C. D., & Chiang, J. C. 1998, *New Astronomy*, 3, 157
 Dermer, C. D., Sturmer, S. J., & Schlickeiser, R. 1997, *ApJS*, 109, 103
 Dermer, C. D. 1998, *ApJ*, 501, L157
 Dermer, C. D., Li, H., & Chiang, J. 1998, in *Third INTEGRAL Workshop*, Taormina, Sicily, in preparation
 Dermer, C. D., Miller, J. A., & Li, H. 1996, *ApJ*, 456, 106
 Feroci, M. et al. 1998, *A&A*, 323, L29

Hartman, R. C., Collmar, W., von Montigny, C., & Dermer, C. D., in *Proceedings of the Fourth Compton Symposium*, ed. C. D. Dermer, M. S. Strickman, & J. D. Kurfess (AIP: New York), 307

Hurley, K. C., et al. 1994, *Nature*, 372, 652

Idesawa, E., et al. 1997, *PASJ*, 49, 631

Kippen, R. M. et al. IAU 6789 (1997)

Kirk, J. G., Rieger, F. M., & Mastichiadis, A. 1998, *A&A*, 333, 452

Kulkarni, S. R. et al. *Nature*, 393 (1998)

Macomb, D. J. et al. 1995, *ApJ*, 449, L99; (e) 1996, *ApJ*, 459, L111

Maraschi, L., Ghisellini, G., & Celotti, A. 1992, *ApJ*, 397, L5

Mattox, J. R. et al. *ApJ*, 476, 692

Melia, F., & Königl, A. 1989, *ApJ*, 340, 162

Mészáros, P., & Rees, M. J. 1992, *ApJ*, 397, 570

Mészáros, P., & Rees, M. J. 1993, *ApJ*, 405, 278

O'Dell, S. L. 1981, *ApJ*, 243, L147

Paczynski, B. 1998, *ApJ*, 494, L45

Panaitecu, A., & Mészáros, P. 1998, *ApJ*, 492, 683

Phinney, E. S. 1982, *MNRAS*, 198, 1109

Piran, T., in *Gamma-Ray Bursts: Second Huntsville Workshop*, eds. G. J. Fishman, J. J. Brainerd, & K. Hurley (AIP: New York), 495

Piro, L., et al. 1998, *A&A*, 331, L41

Rees, M. J., & Mészáros, P., 1992, *MNRAS*, 258, 41P

Sari, R., Piran, T., & Narayan, R. 1998, 497, L17

Sembay, S., et al. 1993, *ApJ*, 404, 112

Takahashi, T., et al. 1996, *ApJ*, 470, L89

Urry, C. M., & Padovani, P. 1995, *PASP*, 107, 803

Urry, C. M., et al. 1997, *ApJ*, 486, 799

Vermeulen, R. C., & Cohen, M. H. 1994, *ApJ*, 430, 467

Vietri, M. 1997, *ApJ*, 478, L9

Vietri, M. 1997, *PRL* 78, 23, 4328

Waxman, E. 1997, *ApJ*, 485, L5

Wijers, R. A. M. J., Rees, M. J., & Mészáros, P. 1997, *MNRAS*, 288, L51

Woosley, S. E. 1993, *ApJ*, 405, 273